QIRT'2022
10.21611/qirt.2022.2003
16th Quantitative InfraRed Thermography Conference

Modeling and simulation of Pulse thermography: comparison with measurements

by P. Bagavac*, L. Krstulović-Opara* and Ž. Domazet*

* FESB, University of Split, R. Boškovića 32, 21 000 Split, Croatia, petra.bagavac@fesb.hr, opara@fesb.hr, domazet@fesb.hr.

Abstract

Pulse thermography as non-destructive testing method is applied on aluminium specimen with five flat bottom holes and the temperature distribution on the front surface of the specimen is recorded by IR camera. Used experimental setup is modelled by the finite element method. After simulation, temperature decay curve is read for multiple characteristic pixels on the front surface of aluminium specimen. Results are compared.

1. Introduction

Pulse thermography has been widely used as a method for non-destructive testing of machine parts [1 -3]. The method is non-contact and non-intrusive and can be easily applied to both small and large work pieces. Applicability and repeatability to polymer materials [4, 5], composite materials [6, 7] and metals [8, 9] has been proven. In this research, the experimental setup of pulse thermography will be modelled by the finite element method. The model will be validated by comparing the actual temperature distribution measurements on the aluminium specimen with the simulation results in multiple characteristic points on specimen surface.

2. Pulse thermography

Pulse thermography is one of active infrared non-destructive methods. Used IR camera is middle wave cooled FLIR SC 5000 and external heat source is Xenon flash lamp able to emit $6000\,J$ in $1/440$ seconds. Front surface of aluminium specimen is covered with black paint coat with high emissivity ($\varepsilon = 0.95$). Experimental set-up is shown in the Fig. 1.a. The drawing of the aluminium specimen is shown in the Fig. 1.b. The overall specimen dimensions are $200x200x10\ mm$. Five flat bottom holes (FBH) were milled on the back surface of the specimen. Each FBH has diameter of $40\ mm$ and varying depth of 2, 3.5, 5, 6.5 and $8\ mm$, respectively. Acquisition frequency is $100\ Hz$ and recording time

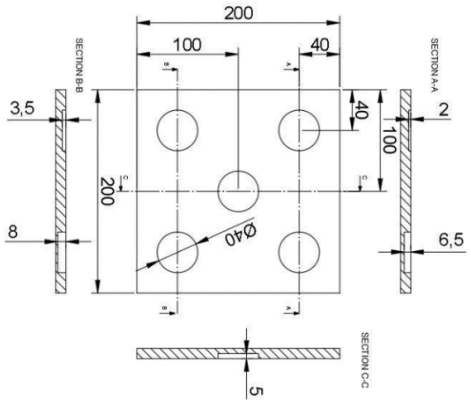

interval is $10\ s$. Sequence of 1000 thermal images is recorded.

Fig.1. *a) Experimental setup: b) aluminium specimen drawing*

are

decay

Fig.

In first column at Fig.2. maximum thermal contrast thermal images are shown. On every thermal image two areas marked, one corresponding to defected zone, and second corresponding to sane zone. For every thermal image, thermal curve for selected pixels is given on the right (second column in 2.). As aluminium is excellent thermal conductor, and

surrounding air is thermal isolator, it is expected that surface upon damaged areas will longer stay wormer.
As expected, maximum thermal contrast is achieved on top of the deepest hole, with depth of 8 mm (Fig. 2.a., top right corner). On thermal image, two characteristic pixels are selected: one in the middle of defected area (x_d, y_d), and second on sane (x_s, y_s) area. In Fig. 2.b are shown thermal decay curves for selected pixels: red curve is for pixel selected on top of the damaged area, and blue curve is for pixel selected on top of sane area. Sane area is chosen near the defected area, so that the effect of uneven heating is kept to a minimum. Useful part of recorded sequence is middle part, from first thermal image recorded after saturation to the last thermal image recorded in time when thermal balance is achieved. As shown on thermal decay curve, thermal balance is achieved after approximately 3 seconds.
For shallower FBH, chosen sane area remained the same. As the distances between damaged and sane pixels increased, effect of uneven heating increased too. As we see in the Fig. 2.c - 2.f, as the depth of the hole decreases, the maximum thermal contrast on the cooling curve also decreases. For shallowest holes, Fig. 2.g – 2.j., not enough thermal contrast is achieved.

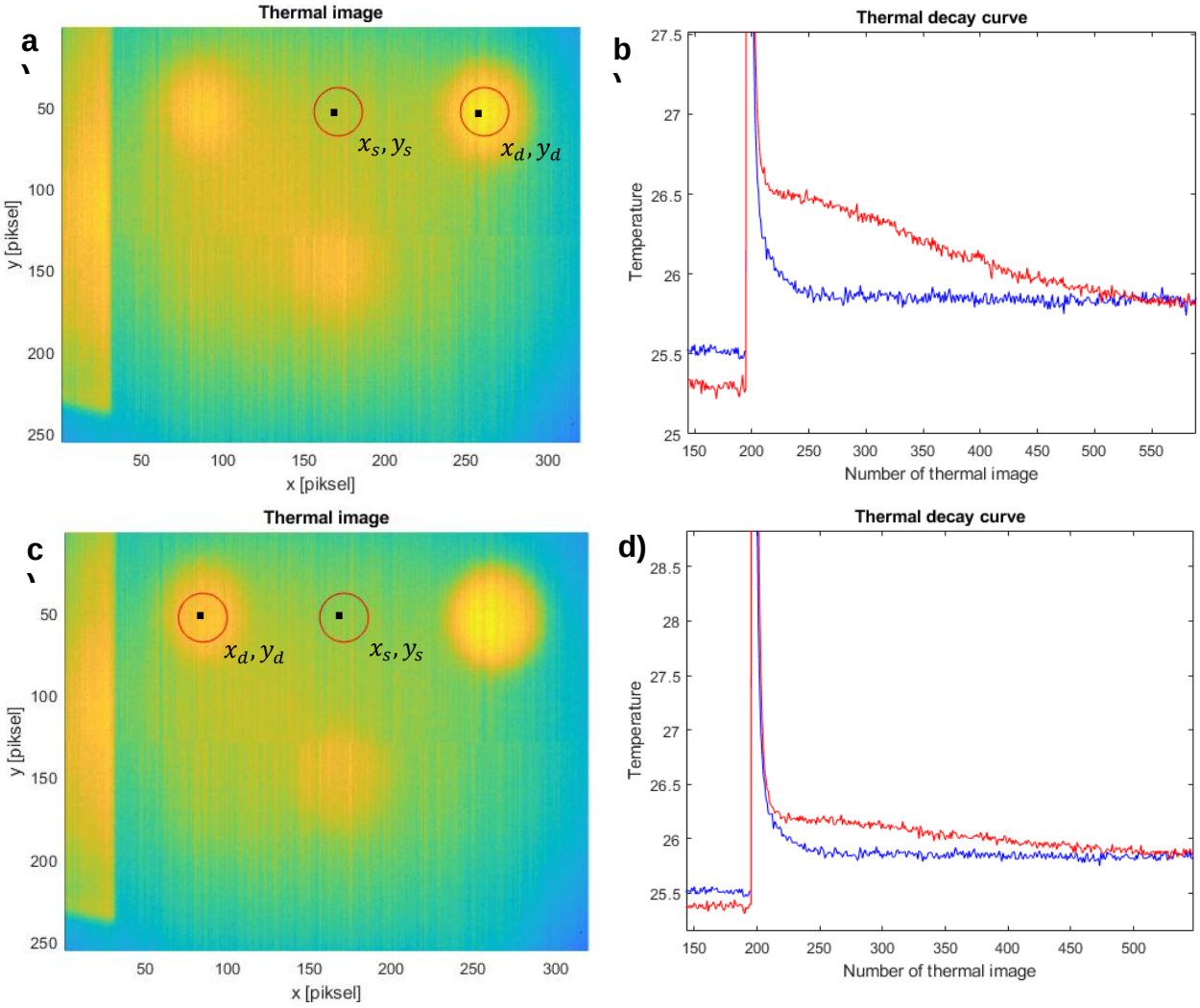

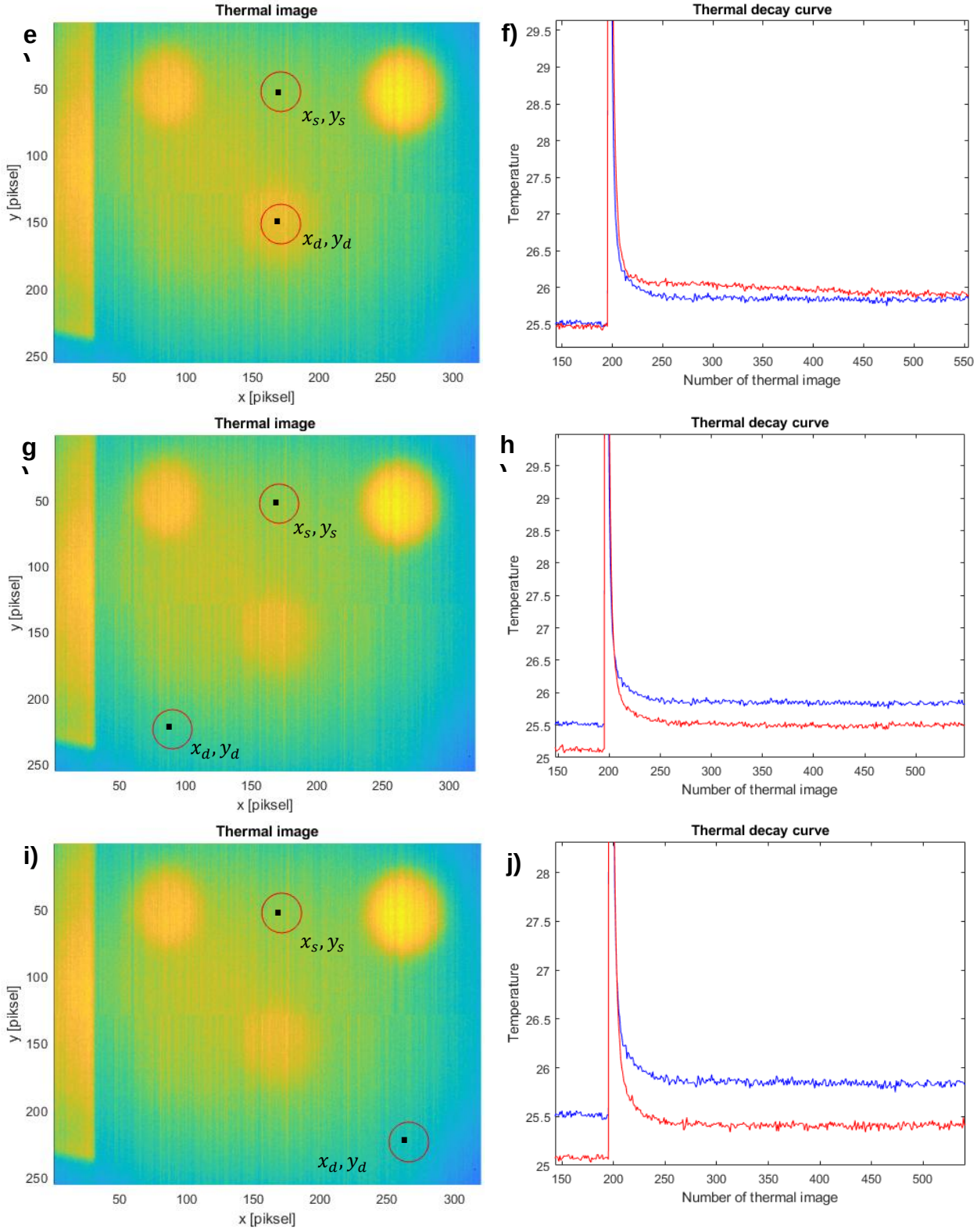

Fig. 2. *First column – maximum thermal contrast thermal image; second column – thermal decay curves*

In Fig. 3. temperature distribution for $y = 53$ is shown. Line is crossing two out of five FBH, with depth of 6.5 and $8\ mm$, respectively. On temperature profile (Fig. 3.b.) both holes have major temperature contrast compared to surface temperature. Temperature profile can be used for quantitative analysis of the size of the damaged area, since from the points of inflection of the temperature profile we can read the diameters of the damage.

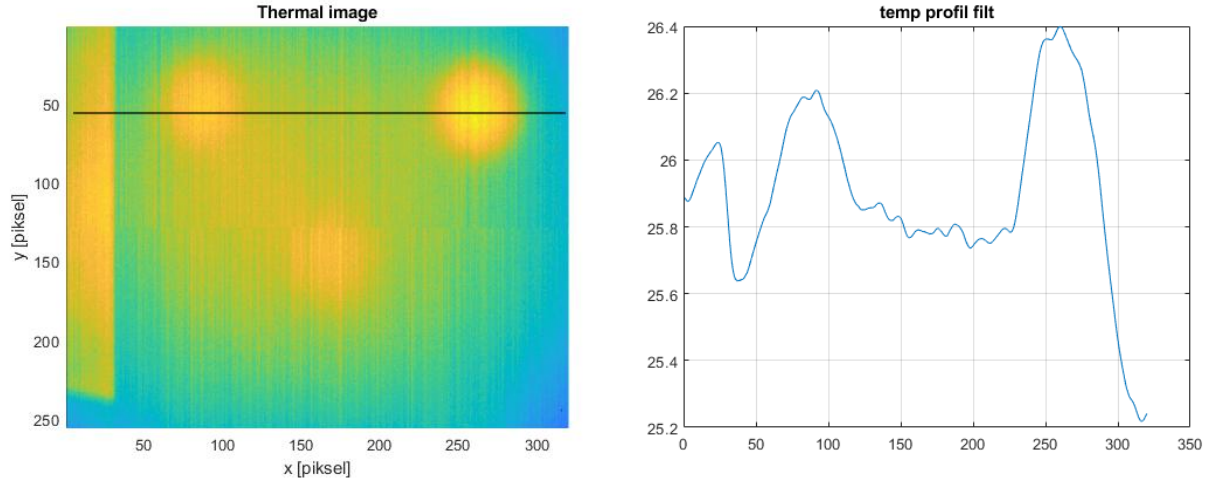

Fig. 3. *Temperature distribution for line y=53*

A finite element model was made according to this procedure of testing. The model was valorised by comparing multiple measurements and simulations.

3. Model configuration

Finite element model consists of two domains, air and aluminium specimen, as shown at Fig. 4.a. A tetrahedral meshing was adapted with average element size of $0.2\ mm$. Properties of the mesh are given at Fig. 4.b. Energy transfer is described by conduction, convection and radiation, more about the used heat transfer equations is given in the literature [10]. When defining the initial conditions, the environment has the properties of air (real gas). The specimen is made of aluminium alloy 6060. The density of the alloy $\rho = 2.70\ g/cm3$, the coefficient of thermal conductivity $k = 210\ W/mK$ and the specific heat capacity $cp = 898\ J/kgK$ are known. The initial temperature is room temperature, $T = 294\ K$. The pressure is atmospheric. The air flow speed is $0.1\ m/s$, which corresponds to the stagnant air in the room. Heat flux is given on one surface (flash unit). The given heat flux is a time-varying function and describes the heat pulse in a real test. The junction of different domains was created as an interface that transfers energy from the surrounding fluid to the aluminium specimen and from the aluminium specimen to the surrounding fluid. The heat transfer parameters are set on the specimen surface. The convection coefficient between the stationary air and the aluminium surface for temperature differences up to $10\ K$ is $5\ W/m2K$. The emissivity coefficient of the specimen is set to 0.95 since the aluminum specimen is painted black of known emissivity. The background emissivity coefficient on the specimen was set at 0.75, which corresponds to the mean emissivity coefficient.

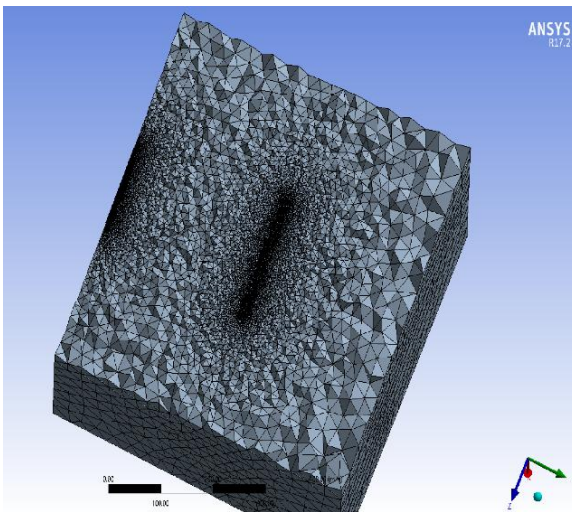

Bodies	2
Active Bodies	2
Nodes	568422
Elements	3173452
Mesh Metric	Skewness
Min	5.594593E-06
Max	0.799770
Average	0.214180
Standard Deviation	0.114738

Fig. 4. *a) Finite element mesh; b) mesh details*

4. Results

Fig. 5. and Fig. 6. shows the temperature distribution on the specimen surface over time $t = 0\,s$, $t = 0.1\,s$, $t = 0.2\,s$, $t = 0.5\,s$, $t = 1\,s$, $t = 2s$, $t = 3.5\,s$, $t = 5\,s$ calculated from finite element model and measured by IR camera, respectively. By comparing the thermal images during cooling time, we can see that finite element model and the response of the actual specimen to the heat flow recorded by the IR camera are following the same behavior of temperature decay. Significant noise levels are present in the thermal images recorded by the IR camera, as these images are not subjected to signal processing.

The Fig. 7. shows the cooling curves for characteristic pixels (FEM) and in given time interval, the sampling frequency of the data is $50\,\mathrm{Hz}$. All cooling curves reach thermal equilibrium in about 3 seconds (150 time steps). The maximum temperature contrast achieved for the deepest damage is $2\,℃$ (from $301\,\mathrm{K}$ to $299\,\mathrm{K}$). The Fig. 8. shows the cooling curves for characteristic pixels (IR measurements) and in given time interval, the sampling frequency of the data is $100\,\mathrm{Hz}$. All cooling curves reach thermal equilibrium in about 3 seconds (300 time steps). The maximum temperature contrast achieved for the deepest damage is $2\,℃$ (from $28\,℃$ to $26\,℃$). FEM model describes the actual measurement very well.

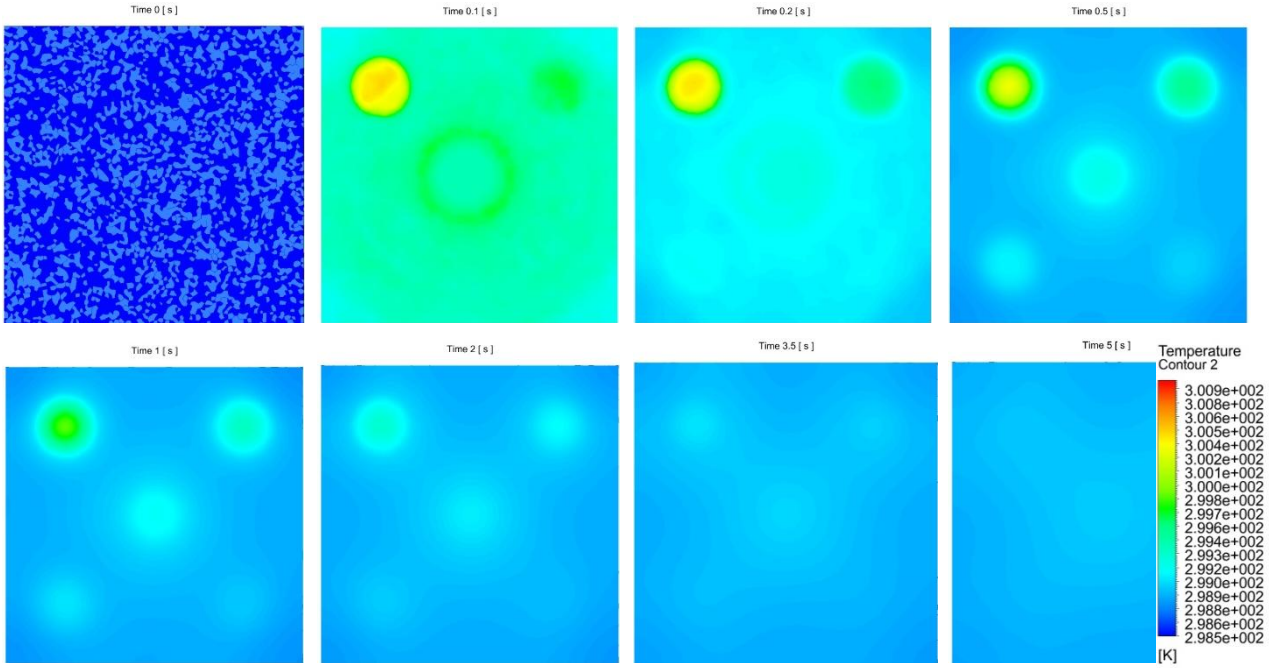

Fig. 5. *Temperature distribution on the front surface of specimen (Ansys): a) t=0 s; b) t=0.05 s; c) t=0,1 s; d) t= 0.5 s; e) t=1 s; f) t=2 s; g) t=3.5 s; h) t=5 s*

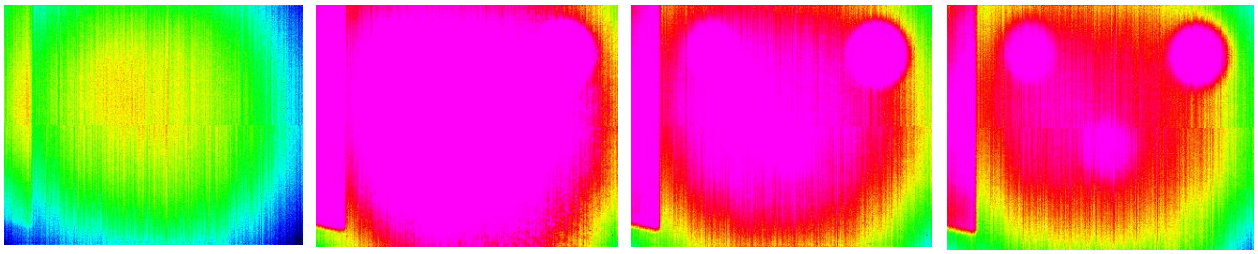

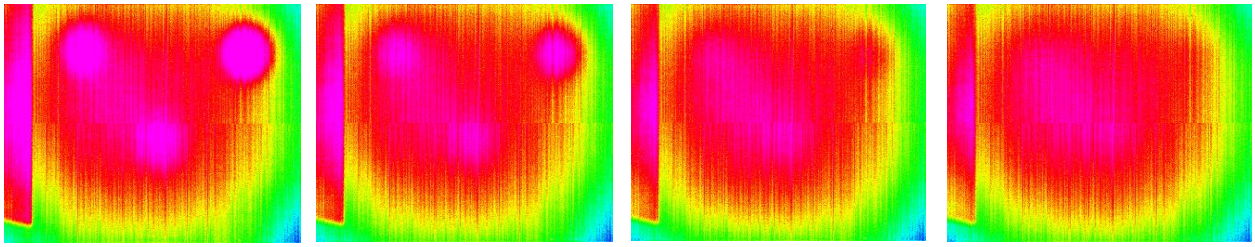

Fig. 6. *Temperature distribution on the front surface of specimen (FLIR): a) t=0 s; b) t=0.05 s; c) t=0,1 s; d) t= 0.5 s; e) t=1 s; f) t=2 s; g) t=3.5 s; h) t=5 s*

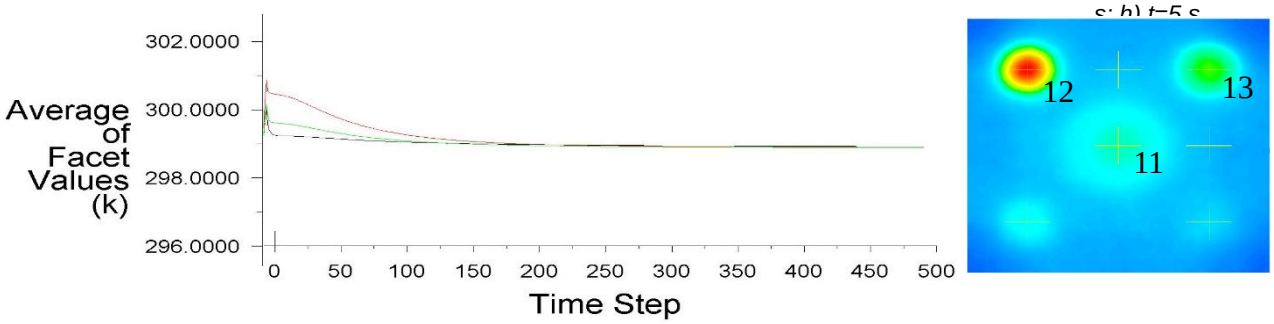

Fig. 7. *Cooling curves for characteristic pixels (FEM)*

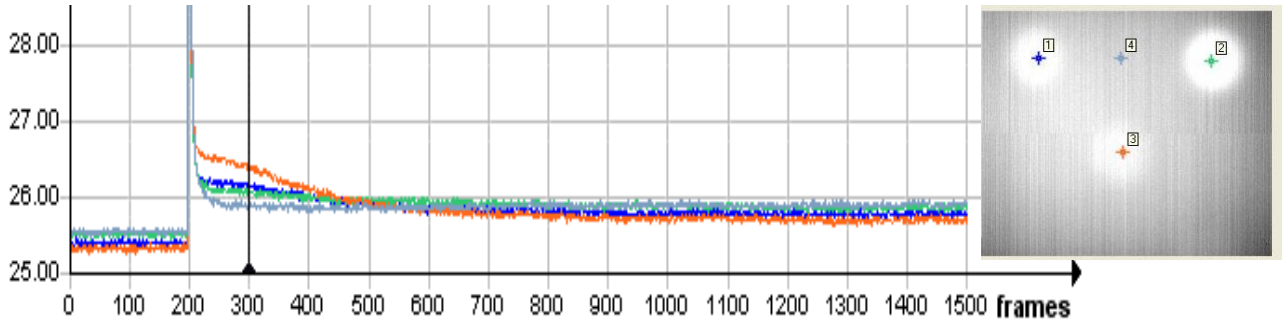

Fig. 8. *Cooling curves for characteristic pixels (IR mesaurements)*

Validation of the finite element model is key step for optimization implementation. The finite element model will be associated to the multy-disciplinary optimization package. In the optimization process, thermal coefficient will be set as optimization variable (e.g., thermal diffusivity), and the target function will be the minimum deviation between the cooling curves of the model and the measurement. In this way, it will be possible to estimate the thermal coefficients in a non- conventional way.

5. Conclusions

In this research, pulse thermography was modelled with finite element method. Experiment modelling can be used to define acquisition parameters from thermal decay curve. It is possible to determine the time at which the specimen will regain thermal equilibrium with the environment after external excitation for the selected material and specimen dimensions.

In future research, this finite element model will be used to evaluate the thermal properties of material for known geometry of specimen.

REFERENCES

[1] X. P. Maldague. Theory and practice of infrared technology for nondestructive testing. John Wiley & Sons, N.Y.,2001
[2] Ibarra-Castanedo, X. Maldague. Pulsed Phase Thermography Reviewed. QIRT J., 1(1): p. 47-70, 2004
[3] Ibarra-Castanedo, X. Maldague. Defect depth retrieval from pulsed phase thermographic data on Plexiglas and aluminum samples. Article in Proceedings of SPIE - The International Society for Optical Engineering, April 2004, DOI: 10.1117/12.540855

[4] G. Busse. Nondestructive evaluation of polymer materials. NDT&E International, 27(5), p. 253–262, 1994
[5] Lj. Tomić, V. Damnjanović, G. Dikić, B. Milovanović. Recostruction of Simulated Cylindrical Defects in Acrylic Plate Using Pulsed Phase Thermography. Applied Science, vol 9. 1854, 2019, DOI:10.3390/app9091854
[6] Petra Bagavac, Lovre Krstulović-Opara, Željko Domazet Enhancing IR Thermographic Inspection of Subsurface Defects by Using the Technique of Edge Detection. Russian Journal of Nondestructive Testing. 57(7): p.609618,2021; DOI:10.1134/S1061830921070020
[7] V. Vavilov, G. Xingwang, S. Wei and L. Yingtao. Peculiarities of detecting Teflon defect surrogates in CFRP by transient IR thermography. DOI: 10.21611/qirt.2004.019
[8] V Vavilov, T Ahmed, J Jin, R.L. Thomas et L.D. Favro. Experimental thermal tomography of solids by using the flash one-side heating. Sov. J. NDT, 12, 1990.
[9] Petra Bagavac, Lovre Krstulović-Opara, Željko Domazet. Infrared Thermography of Steel Structure by FFT, Materials Today: Proceedings, 12 (2): p. 298-303, 2019, https://doi.org/10.1016/j.matpr.2019.03.127.
[10] ANSYS, Inc. (2016) ANSYS Fluent User's Guide, Release 17.2.